Graphene based low insertion loss electro-absorption modulator on SOI waveguide

Muhammad Mohsin,[1,*] Daniel Schall,[1] Martin Otto,[1] Achim Noculak,[2] Daniel Neumaier,[1] and Heinrich Kurz[1]

[1]*Advanced Microelectronic Center Aachen (AMICA), AMO GmbH, Otto-Blumenthalstr. 25, 52074 Aachen, Germany*
[2]*Chair of High Frequency Electronics, RWTH University Aachen, Sommerfeldstr. 24, 52074 Aachen, Germany*
**mohsin@amo.de*

Abstract: Graphene is considered a promising material for broadband opto-electronics because of its linear and gapless band structure. Its optical conductivity can be significantly tuned electrostatically by shifting the Fermi level. Using mentioned property, we experimentally demonstrate a graphene based electro-absorption modulator with very low insertion loss. The device is realized on a silicon on insulator (SOI) waveguide operating at 1550 nm wavelength. The modulator shows a modulation depth of 16 dB and an insertion loss of 3.3 dB, surpassing GeSi and previous graphene based absorption modulators and being comparable to silicon Mach-Zehnder interferometer based modulators.

OCIS codes: (130.0250) Optoelectronics; (250.7360) Waveguide modulators; (160.2100) Electro-optical materials.

References and links

1. G. T. Reed, G. Mashanovich, F. Y. Gardes, and D. J. Thomson, "Silicon optical modulators," Nat. Photonics **4**(8), 518–526 (2010).
2. P. Chaisakul, D. Marris-Morini, M. S. Rouifed, J. Frigerio, D. Chrastina, J. R. Coudevylle, X. Le Roux, S. Edmond, G. Isella, and L. Vivien, "Recent progress in GeSi electro-absorption modulators," Sci. Technol. Adv. Mater. **15**(1), 014601 (2014).
3. X. Xiao, H. Xu, X. Li, Z. Li, T. Chu, J. Yu, and Y. Yu, "60 Gbit/s silicon modulators with enhanced electro-optical efficiency," in Optical Fiber Communication Conference (Anaheim, Calif., 2013).
4. K. S. Novoselov, A. K. Geim, S. V. Morozov, D. Jiang, Y. Zhang, S. V. Dubonos, I. V. Grigorieva, and A. A. Firsov, "Electric field effect in atomically thin carbon films," Science **306**(5696), 666–669 (2004).
5. K. S. Novoselov, A. K. Geim, S. V. Morozov, D. Jiang, M. I. Katsnelson, I. V. Grigorieva, S. V. Dubonos, and A. A. Firsov, "Two-dimensional gas of massless Dirac fermions in graphene," Nature **438**(7065), 197–200 (2005).
6. Y. Zhang, Y. W. Tan, H. L. Stormer, and P. Kim, "Experimental observation of the quantum Hall effect and Berry's phase in graphene," Nature **438**(7065), 201–204 (2005).
7. A. B. Kuzmenko, E. van Heumen, F. Carbone, and D. van der Marel, "Universal optical conductance of graphite," Phys. Rev. Lett. **100**(11), 117401 (2008).
8. Q. Bao and K. P. Loh, "Graphene photonics, plasmonics, and broadband optoelectronic devices," ACS Nano **6**(5), 3677–3694 (2012).
9. M. Liu, X. Yin, E. Ulin-Avila, B. Geng, T. Zentgraf, L. Ju, F. Wang, and X. Zhang, "A graphene-based broadband optical modulator," Nature **474**(7349), 64–67 (2011).
10. J. Gosciniak and D. T. H. Tan, "Theoretical investigation of graphene-based photonic modulators," Sci Rep **3**, 1897 (2013).
11. M. Liu, X. Yin, and X. Zhang, "Double-Layer graphene optical modulator," Nano Lett. **12**(3), 1482–1485 (2012).
12. X. Li, W. Cai, J. An, S. Kim, J. Nah, D. Yang, R. Piner, A. Velamakanni, I. Jung, E. Tutuc, S. K. Banerjee, L. Colombo, and R. S. Ruoff, "Large-area synthesis of high-quality and uniform graphene films on copper foils," Science **324**(5932), 1312–1314 (2009).
13. S. J. Koester and M. Li, "Waveguide-Coupled Graphene Optoelectronics," IEEE J. Sel. Top. Quantum Electron. **20**(1), 6000211 (2014).
14. F. Wang, Y. Zhang, C. Tian, C. Girit, A. Zettl, M. Crommie, and Y. R. Shen, "Gate-variable optical transitions in graphene," Science **320**(5873), 206–209 (2008).

#209828 - $15.00 USD Received 9 Apr 2014; revised 23 May 2014; accepted 27 May 2014; published 13 Jun 2014

15. M. Streshinsky, R. Ding, Y. Liu, A. Novack, Y. Yang, Y. Ma, X. Tu, E. K. S. Chee, A. E. J. Lim, P. G. Q. Lo, T. Baehr-Jones, and M. Hochberg, "Low power 50 Gb/s silicon traveling wave Mach-Zehnder modulator near 1300 nm," Opt. Express **21**(25), 30350–30357 (2013).
16. A. Castellanos-Gomez, M. Wojtaszek, R. H. M. Smit, N. Tombros, N. Agraït, B. J. van Wees, and G. Rubio-Bollinger, "Electronic inhomogeneities in graphene: the role of the substrate interaction and chemical doping," arXiv:1210.4147 (2012).
17. H. Xu, Y. Chen, J. Zhang, and H. Zhang, "Investigating the mechanism of hysteresis effect in graphene electrical field device fabricated on SiO_2 substrates using Raman spectroscopy," Small **8**(18), 2833–2840 (2012).
18. Y. G. Lee, C. G. Kang, C. Cho, Y. Kim, H. J. Hwang, and B. H. Lee, "Quantitative analysis of hysteretic reactions at the interface of graphene and SiO 2 using the short pulse I-V method," Carbon **60**, 453–460 (2013).
19. H. Wang, Y. Wu, C. Cong, J. Shang, and T. Yu, "Hysteresis of electronic transport in graphene transistors," ACS Nano **4**(12), 7221–7228 (2010).

1. Introduction

Electro-optical modulators are key components for optical communication systems. The most important figures of merit for these devices are operation speed, extinction ratio, insertion loss, energy consumption, and footprint. In integrated silicon photonic systems, the race for the perfect modulator is still open, as none of the actual devices including Mach-Zehnder interferometer (MZI) based modulators, silicon ring modulators or SiGe absorption modulators show sufficient values for all mentioned parameters [1,2]. MZI based modulators show large optical extinction and relatively low insertion loss, but their footprint of order of few millimeters is very large, especially for applications in intrachip communication systems [3]. Silicon micro-ring modulators have a significantly lower footprint, but operate only in a very narrow optical spectrum, making them extremely sensitive to temperature variations and fabrication tolerances [1]. Therefore active tuning systems have to be utilized, increasing device complexity and energy consumption. Another modulator type that is compatible to a CMOS based process flow is the electro-absorption modulator based on SiGe diodes utilizing the Franz-Keldysh effect [2]. These modulators offer very low footprint and broadband operation, but with large insertion loss and high static power dissipation.

Graphene, the two-dimensional carbon allotrope [4–6], shows broadband light absorption ranging from UV to far infrared in its intrinsic state [7] and is thus gaining significance in photonics [8]. When graphene is doped, the absorption is turned-off effectively especially at infrared frequencies by state-filling and corresponding Pauli-blocking. This effect can be used to realize an electro-absorption modulator, where state-filling is tuned by electro-static gating [9]. It has been predicted that such devices have the potential to deliver high speed operation (>100 GHz), broadband operation in the range of 1 to 4 μm wavelength, small footprint of order of μm^2, and low energy consumption (<fJ/bit), which would surpass state-of-the-art devices by far [10]. The minimum insertion loss of graphene based absorption modulators is defined by the interplay between inter- and intraband absorption. Depending on the modulator design, operation wavelength and drive voltage, $\Delta\alpha/\alpha$ values (ratio of extinction ratio to the insertion loss) significantly larger than 10 are conceivable in realistic devices, which would be more than sufficient for most applications [10].

So far, first graphene based modulators have been successfully realized demonstrating principle functionality [9,11]. However their insertion loss, being of the same order or even larger than the extinction ratio, was far behind theoretical predictions and not acceptable for most applications. In this paper, we present a graphene based electro-absorption modulator with 3.3 dB insertion loss and 16 dB modulation amplitude ($\Delta\alpha/\alpha = 4.8$) operating at 1550 nm wavelength on a 520 nm wide SOI waveguide, not only surpassing electro-absorption modulators based on SiGe and graphene, but being competitive to the best silicon MZI.

2. Results

A schematic of the modulator is shown in Fig. 1. A 520 nm wide strip waveguide and grating couplers optimized for 1550 nm were fabricated on 220 nm thick SOI. To smooth the step

#209828 - $15.00 USD Received 9 Apr 2014; revised 23 May 2014; accepted 27 May 2014; published 13 Jun 2014

edges of the waveguide, an HSQ layer was spin-coated and cured. The thickness of the HSQ on top of the waveguide is ~30 nm, while it is ~130 nm on the rest of the

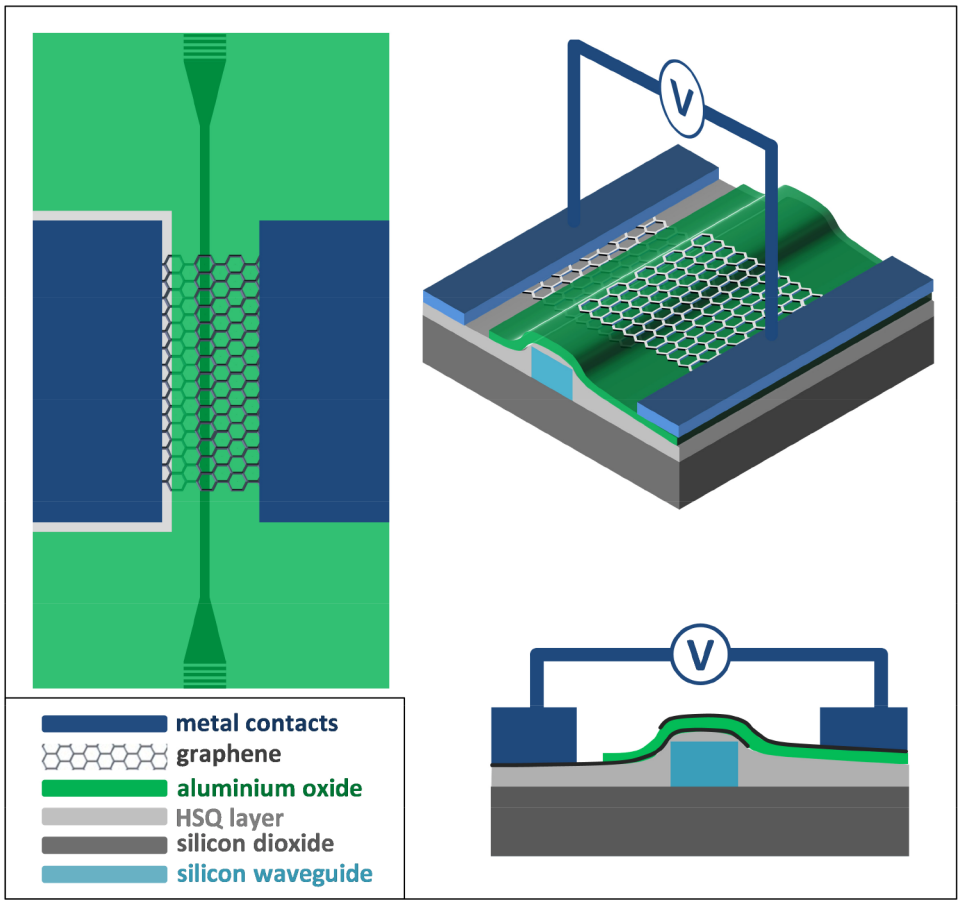

Fig. 1. Top view of device, light was coupled using grating couplers (left). Isometric view of device showing graphene layer on top of Si waveguide (top right). Cross-sectional view of device with graphene layers separated by 94 nm aluminum oxide (bottom right).

chip. Fiber-to-fiber losses at this stage related to the silicon waveguide and the grating couplers are ≈10.0 dB as specified in Fig. 2 as 'initial insertion loss'. A single layer of graphene grown by CVD on copper substrate was transferred to the sample by standard PMMA method [12], contacted by nickel electrode and patterned by oxygen plasma. Proper etching of copper foil is of critical concern during graphene transfer process as the presence of copper particles leads to increased losses. In principle, we have used the same process for graphene transfer as the one used by [11] with the exception that our process is optimized for thorough metal etching thus avoiding transfer of any copper particles, from the copper foil, onto the waveguide. Furthermore, the PMMA/graphene stack was cured at 180°C for 15 minutes after transferring to target substrate, whereas in [11] it was baked overnight (the temperature is not mentioned). A temperature sufficiently higher than glass transition temperature of PMMA (180°C in our case) is required so that the graphene rests perfectly smoothened on top of substrate. This avoids cracking and charge inhomogeneities or localized doping in graphene layer. The PMMA was then removed by rinsing the substrate in hot acetone. The graphene length on the waveguide is 300 μm and the contact is separated by 5 μm from the waveguide. The specific evanescent field absorption for this graphene layer, measured in a separate study using different interaction lengths, was found to be 0.06 dB/μm.

#209828 - $15.00 USD Received 9 Apr 2014; revised 23 May 2014; accepted 27 May 2014; published 13 Jun 2014

After the direct deposition of 94 nm thick Al_2O_3 layer by atomic layer deposition using TMA and water vapor as precursors, a second layer of graphene was transferred to the sample, acting as counter electrode, using the same transfer process as described before. Light absorption in second graphene layer was measured to be significantly smaller (<0.01 dB/μm) compared to the first graphene layer. Though usage of ~90 nm oxide between two graphene layers requires higher operation voltages due to weaker dielectric coupling, it causes significantly low insertion losses as the upper graphene layer is far outside the evanescent field [13]. The overlap area between the two graphene layers is 300μm x 6μm. Contacting and patterning of the second graphene layer were done identical to that of the first layer, with a contact distance of 5 μm from the waveguide. Finally, vias were etched to contact the metal pad of first graphene layer by HF etching.

The basic operation principle of the modulator is as follows: Light transmission through the waveguide is mainly determined by its interaction with the lower graphene layer. In this layer, the electro-chemical potential μ, and thus optical conductance [14], can be controlled electrostatically by applying a voltage at the upper layer graphene, while keeping the lower layer grounded. For this modulator geometry, light absorption in the dominant lower layer is expected to be maximal for voltages where $\mu < hf/2 = \pm 400$ meV (that is half of the photon energy). At voltages where $\mu \geq \pm 400$ meV, the bleaching starts to be operative and the modulator is turned to its on-state. In Fig. 2, the relative fiber-to-fiber transmission of the modulator at 1550 nm wavelength with 1.1 mW input laser power is plotted as a function of applied voltage. As can be seen, light transmission is minimal for voltages ranging from −30 to −10 V for one sweep direction (solid line), indicating a location of the charge neutrality point of the lower graphene layer at −20 V (n-type doping).

At voltages above −10 V and below −30 V the light transmission increases significantly and the modulator is turned in its on-state. The maximum light transmission is −13.3 dB, while the minimum is −29.3 dB, resulting in an optical extinction of 16 dB and an insertion loss of 3.3 dB of the modulator. This results in $\Delta\alpha/\alpha = 4.8$. This value is significantly larger than values in previous graphene (≤1.6) and SiGe based absorption modulators (≤1.5) [2,11], and comparable to the values in Si-MZI based modulators (≤4.3) [15]. For the discrepancy between theoretical limits and actual device performance three distinct reasons are identified: 1) The 94 nm thick Al_2O_3 layer on grating couplers reduces their coupling efficiency. These losses have been measured in a reference experiment, where the same device without graphene was fabricated, to be 0.7 dB. 2) Despite having an optimized process for graphene transfer, some parasitic copper particles are still transferred to the waveguide, increasing the losses. 3) Inhomogeneities in the doping level of the graphene reduce the efficiency of Pauli-blocking [16]. Hence, there are still margins for a further reduction in insertion loss by optimizing the fabrication process and $\Delta\alpha/\alpha > 10$ seems to be realistic.

In quasi-static measurements (Fig. 2), the voltage dependent transmission of the modulator exhibits a strong hysteretic behavior, which is typical for graphene based field effect devices (GFEDs) under ambient conditions. In GFEDs, hysteretic behavior occurs mainly because of charge traps generated by adsorbates, typically O_2/H_2O redox couples, at the graphene/dielectric interface [17,18]. The size of the hysteresis in GFEDs increases with the voltage sweep range and is also maximal at low cycle speeds as performed here [19]. For RF operation hysteretic behavior is not expected. In order to prove the absence of the hysteresis under typical operation conditions the modulator was driven with a sine-wave signal at 50 MHz with peak-to-peak voltage swing of 6 V. The optical output signal of the modulator (inset of Fig. 3) shows an excellent sine-wave characteristic proving not only hysteresis free operation, but also linear response for these operation conditions. The corresponding optical modulation amplitude was 10 μW, which is close to the maximum value obtained from the DC transmission characteristic (15 μW for 6 V drive voltage and 1.1 mW optical input power).

#209828 - $15.00 USD Received 9 Apr 2014; revised 23 May 2014; accepted 27 May 2014; published 13 Jun 2014

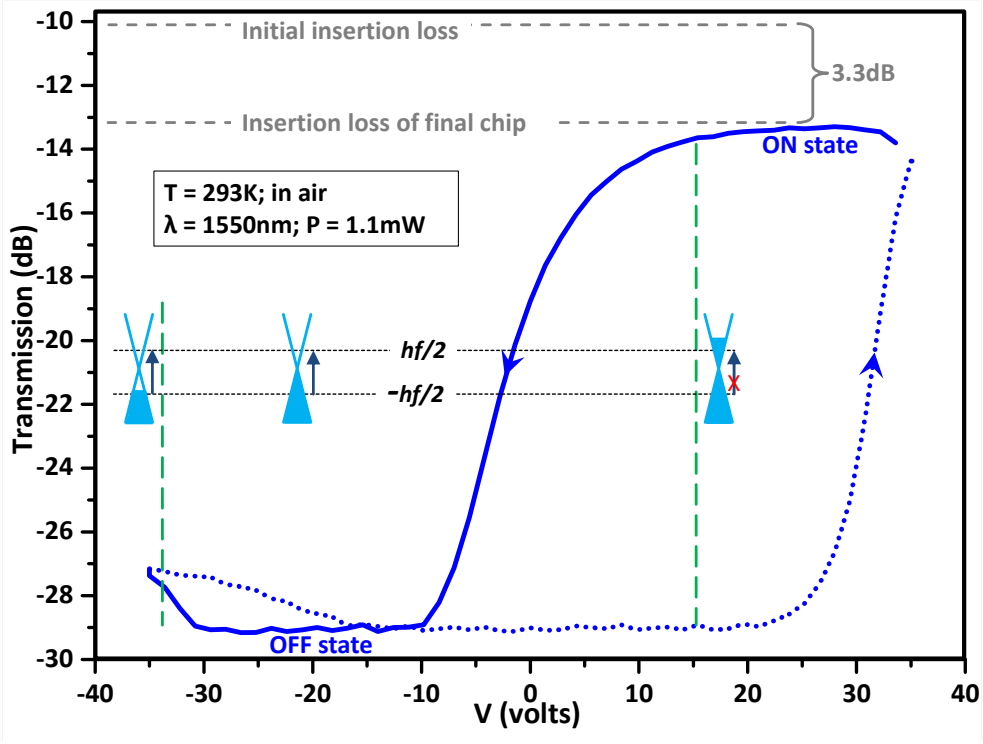

Fig. 2. Static measurement of the optical transmission as a function of applied voltage for both sweep directions. The location of Fermi energy of the lower graphene layer is indicated for one sweep directions to illustrate the operation principle.

Measurements of the frequency dependent electro-optical response have been performed using a network analyzer and a photodiode calibrated up to 1.8 GHz. The corresponding electro-optical response is shown in Fig. 3, giving a f_{-3dB} bandwidth of 670 MHz. Note that the two dips in the spectrum at 320 MHz and 850 MHz are artifacts from the experimental setup. For our device layout, the actual bandwidth is limited by device capacitance and access resistance, defining a RC low pass, where $f_{-3dB} = 1/(2\pi RC)$ [10]. A corresponding first order low pass characteristic is fitted to the experimental data (red line in Fig. 3). Using the measured device capacitance of 2.3 pF a device resistance of 105 Ω is extracted. This device resistance value can be explained well using the device geometry, a specific graphene resistance of ~2 kΩ/sq and a contact resistance of ~5 kΩμm. Similar values have been obtained on reference TLM structures using the same fabrication process. The device layout has not been designed for high speed operation in this study. Hence, a reduction of the overlap of the two graphene layers to reduce C and a reduction of the distance of the contacts to the waveguide to reduce R (the actual values are 6 μm and 5 μm, respectively), has the potential to significantly increase f_{-3dB}, making this device concept competitive not only in terms of insertion loss but also in terms of operation speed.

#209828 - $15.00 USD Received 9 Apr 2014; revised 23 May 2014; accepted 27 May 2014; published 13 Jun 2014

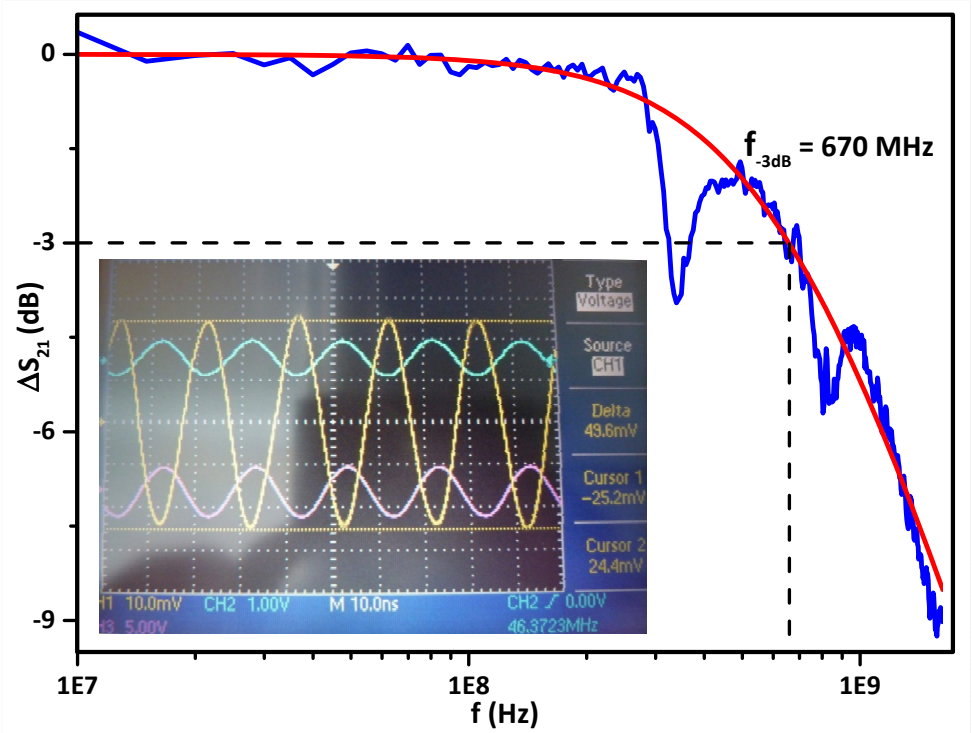

Fig. 3. Relative electro-optical response of the modulator as a function of frequency. f_{-3dB} is 670 MHz. The inset shows the output signal of the modulator at 50 MHz (yellow line) for an AC input voltage V_{PP} = 6 V (purple and cyan lines represent the reference signals).

3. Conclusions

While the huge potential of graphene based absorption modulators has been predicted and already partially proven [9–11], it was so far unclear if competitive insertion loss can be achieved in real devices. By demonstrating a functional graphene based electro-absorption modulator with only 3.3 dB insertion loss at 16 dB optical extinction, we show that also for this figure of merit graphene based electro-absorption modulators are competitive to state-of-the-art modulators. Hence, graphene based electro-absorption modulators could become the perfect solution especially for intrachip communication systems and sensor applications, where low footprint and large spectral bandwidth are extremely important.

Acknowledgments

This work was financially supported by European Commission under Contract No. 285275 (”Grafol”) and by the German Science Foundation DFG within the SPP 1459 Graphene (Project ”GraTiS”). The silicon waveguides were fabricated within the ePIXnet network of excellence.

#209828 - $15.00 USD Received 9 Apr 2014; revised 23 May 2014; accepted 27 May 2014; published 13 Jun 2014